Thermochimica Acta 512 (2011) 258–267

Contents lists available at ScienceDirect

Thermochimica Acta

journal homepage: www.elsevier.com/locate/tca

Thermodynamic description of the Al–Cu–Mg–Mn–Si quinary system and its application to solidification simulation

Keke Chang[a], Shuhong Liu[a,b], Dongdong Zhao[a], Yong Du[a,b,*], Liangcai Zhou[a], Li Chen[a,b]

[a] State Key Laboratory of Powder Metallurgy, Central South University, Hunan 410083, PR China
[b] Science Center for Phase Diagrams & Materials Design and Manufacture, Central South University, Hunan 410083, PR China

ARTICLE INFO

Article history:
Received 24 September 2010
Received in revised form 26 October 2010
Accepted 2 November 2010
Available online 11 November 2010

Keywords:
Al–Cu–Mg–Mn–Si
CALPHAD approach
First-principles calculations
Solidification
Al alloys

ABSTRACT

By means of the first-principles calculations, the enthalpy of formation for the quaternary phase in the Al–Cu–Mg–Si system was computed. A set of self-consistent thermodynamic parameters for the Al–Cu–Mg–Si and Al–Cu–Mn–Si systems was then obtained using CALPHAD approach taking into account the reliable experimental data and the first-principles calculations. The thermodynamic database for the Al–Cu–Mg–Mn–Si system was developed based on the constituent binary, ternary, and quaternary systems. Comprehensive comparisons between the calculated and measured phase diagrams and invariant reactions showed that the experimental information was satisfactorily accounted for by the present thermodynamic description. The obtained database was used to describe the solidification behavior of Al alloys B319.1 (90.2Al–6Si–3.5Cu–0.3Mg, in wt.%) and B319.1 + *x*Mn (*x* = 0.5–2, in wt.%) under Gulliver–Scheil non-equilibrium condition. The reliability of the present thermodynamic database was also verified by the good agreement between calculation and experiment for Gulliver–Scheil non-equilibrium solidification.

1. Introduction

Al alloys are widely used in packaging, automotive and aircraft industries. Addition of the alloying elements, such as Cu, Mg and Si [1,2], can improve the mechanical and chemical properties of Al alloys. Large amounts of studies have been performed on the Al–Cu–Mg–Si alloys due to the application prospects in the automotive industry [3–7]. It is found that the addition of Mn will yield an increase in strength of the Al–Cu–Mg–Si alloys [8]. Thus, Al–Cu–Mg–Si alloys with Mn addition (or Al–Cu–Mg–Mn–Si alloys) attract increasing interests [9–12].

The mechanical and chemical properties as well as the corrosion resistance of solidified Al alloys are heavily dependent on the microstructure obtained after solidification [13,14]. Accurate predictions of reactions during solidification are essential to design solidification process and subsequent heat treatments in order to obtain optimal material properties. Consequently, information on the phase equilibria and thermodynamic properties of the Al-based alloy systems is of great importance, especially for the multi-component systems [15].

The CALPHAD (CALculation of PHAse Diagrams) approach has become a valuable tool in the calculation of complex, multi-component phase equilibria of industrial alloys based on experimental thermodynamic and phase diagram data. It has been demonstrated by Wolverton et al. [16] that the first-principles calculations provide a method of predicting thermodynamic data when such data are not available in the literature. This method has been verified to be reliable due to the good agreement between the first-principles calculated enthalpies of formation and the experimental data [17–19]. Thus, it is reasonable and important to apply the first-principles calculations to the present thermodynamic modeling, because no thermodynamic data for the quaternary phase in the Al–Cu–Mg–Si system are available in the literature up to now.

The aims of the present work are to (1) obtain the enthalpy of formation for the quaternary phase in the Al–Cu–Mg–Si system from the first-principles calculations in order to provide a reliable energy basis for the thermodynamic modeling; (2) establish a thermodynamic database for the quinary Al–Cu–Mg–Mn–Si system on the basis of the constituent binary, ternary and quaternary systems using the CALPHAD approach; and (3) apply the present database to solidification simulation of Al alloys B319.1

* Corresponding author at: State Key Laboratory of Powder Metallurgy, Central South University, Changsha, Hunan 410083, PR China. Tel.: +86 731 88836213; fax: +86 731 88710855.
E-mail address: yongducalphad@gmail.com (Y. Du).

0040-6031/$ – see front matter © 2010 Elsevier B.V. All rights reserved.
doi:10.1016/j.tca.2010.11.009

Table 1
List of the symbols to denote the phases in Al-rich corner investigated in the present work.

Symbol	Phase
L	Liquid
(Al)	Solid solution based on fcc_A1 Al
(Si)	Solid solution based on diamond_A4 Si
β-AlMg	Binary phase $Al_{140}Mg_{89}$
Al_6Mn	Binary phase Al_6Mn
$Al_{12}Mn$	Binary phase $Al_{12}Mn$
Mg_2Si	Binary phase Mg_2Si
θ	Binary phase Al_2Cu
τ_1-AlCuMn	Ternary compound $Al_{28}Cu_7Mn_4$
τ_4-AlCuMn	Ternary compound $Al_5Cu_2Mn_3$
τ_9-AlMnSi	Ternary compound $Al_{14}Mn_4(Al,Si)_5$
S	Ternary compound Al_2CuMg
T-AlCuMg	Ternary compound Al $Mg_{26}(Al,Mg)_6(Al,Cu,Mg)_{48}$
Q	Quaternary phase in the Al–Cu–Mg–Si system

Table 2
Comparison of the calculated and measured invariant reaction temperatures for Al-rich parts of the Al–Cu–Mg system.

Reaction	Measured T (°C)	Calculated T (°C)
L ↔ (Al) + θ + S	502 [68] 506 [69] 507 [70]	502 (this work)
L + S ↔ (Al) + T-AlCuMg	470 [68] 467 [69] 468 [70]	469 (this work)
L ↔ (Al) + T-AlCuMg + β-AlMg	451 [68] 451 [69] 443 [70]	448 (this work)

(90.2Al–6Si–3.5Cu–0.3Mg, in wt.%) and B319.1 + xMn (x = 0.5–2, in wt.%).

2. Evaluation of phase diagram information in the literature

In order to facilitate reading, information on the phases in Al-rich corner investigated in the present work is listed in Table 1.

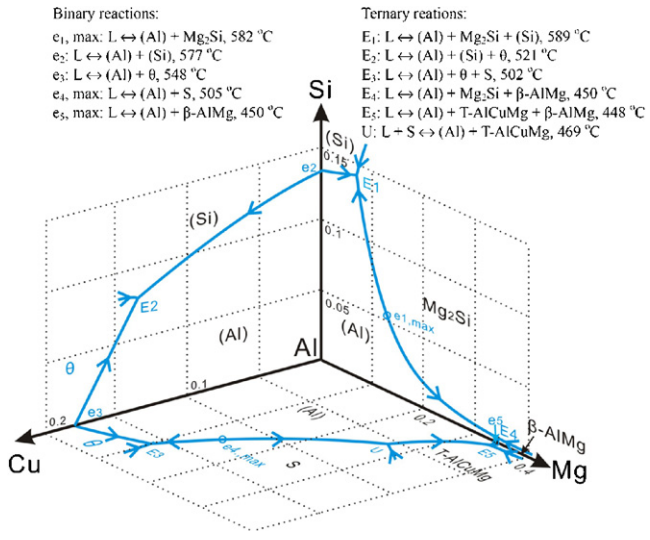

Fig. 1. Calculated liquidus projections of the Al–Cu–Mg, Al–Cu–Si [32] and Al–Mg–Si [33] systems in the Al-rich corner. The compositions are given in weight fractions.

2.1. The binary systems

The thermodynamic parameters of the 10 binary systems in the quinary system: Al–Cu [20], Al–Mg [21], Al–Mn [22], Al–Si [23], Cu–Mg [24], Cu–Mn [25], Cu–Si [26], Mg–Mn [27], Mg–Si [28] and Mn–Si [29], are adopted in the present thermodynamic database.

2.2. The ternary systems

The thermodynamic parameters for the Al–Cu–Mg and Cu–Mg–Si systems in COST 507 project [20] are accepted in the present work. However, the published parameters cannot describe the experimental phase equilibria in the Al-rich corner of the ternary Al–Cu–Mg system accurately [30]. In the present work, the thermodynamic parameter for the fcc_A1 phase in the Al–Cu–Mg system is thus reassessed in order to describe the phase equilibria in the Al-rich corner of the system [30].

The thermodynamic data sets for the Al–Cu–Mn (shown in Supplementary Table 1), Al–Cu–Si, Al–Mg–Mn, Al–Mg–Si, Al–Mn–Si, and Cu–Mn–Si (shown in Supplementary Table 2) are taken from He [31], He et al. [32], Du et al. [22], Feufel et al. [33], Du et al. [34] and Liu [35], respectively.

The remaining two ternary systems Cu–Mg–Mn and Mg–Mn–Si are assumed to behave as ideal solutions, i.e. their thermodynamic parameters are synthesized from the corresponding sub-binary sides.

2.3. The quaternary systems

2.3.1. The Al–Cu–Mg–Si system

The phase diagram data in the Al-rich corner of the quaternary Al–Cu–Mg–Si system have been the subject of numerous studies [36–42]. Using thermal analysis (TA) and optical microscopy (OM), Petrov and Nagorskaya [36] investigated the phase equilibria on the quaternary system with the composition of 90, 80, 70, 60, and 50 wt.% Al. Axon [37–39] measured the isothermal sections at 460 °C with the compositions of Si at 0.6, 1.2 and 2 wt.% by means of metallographic examination, Willey [40] reported one isothermal section with 92 wt.% at 460 °C, which is consistent with the results from Axon [37–39]. By means of optical microscopy, Smith [30] investigated the phase equilibria at 500 °C in the composition ranges of 0–4.5 wt.% Cu, 0–4 wt.% Mg and 0–2 wt.% Si. Also, Crowther [41] reported one vertical section from 4 wt.% Cu, 4 wt.% Mg to 4 wt.% Cu, 4 wt.% Si. Recently, Zolotorevsky et al. [42] constructed one isothermal section at 500 °C with 9 wt.% Si and two vertical sections with a fixed value of 3 wt.% Cu–9 wt.% Si and 1 wt.% Mg–10 wt.% Si. All the above experimental data are considered in the present thermodynamic modeling.

Three eutectic and three peritectic invariant reactions in the Al-rich corner were firstly reported by Petrov and Nagorskaya [36]. These reactions were reexamined by Schrader [43] and Mondolfo [44], whose results are in agreement with the data reported by Petrov and Nagorskaya [36] except for the invariant reaction L + Mg_2Si ↔ Q + (Al) + (Si). The reaction temperature 521 °C [36] was observed by Schrader [43] to be 541.6 °C. Subsequently, the above reaction was determined to be L + (Si) + Mg_2Si ↔ Q + (Al) at 529 °C [44]. Mondolfo's results [44] are accepted in the assessment work of Belov et al. [12] and Zolotorevsky et al. [42]. Other researchers [6,45–49] also studied the invariant reactions in the Al-rich corner and their results are consistent with those of Mondolfo [44]. Thus, the experimental data on the invariant reactions from Mondolfo [44] are used in the present optimization.

The quaternary phase in the Al–Cu–Mg–Si system was firstly observed and designated as the AlCuMgSi phase by Dix et al. [50]. The phase has then been named as Q [37–39,43–45], W [36], λ [46] and h-AlCuMgSi [51,52]. The structure of Q has been reported

Table 3
Summary of the optimized thermodynamic parameters in the Al–Cu–Mg–Mn–Si system.[a]

Q: $Al_{3/21}\ Cu_{2/21}\ Mg_{9/21}\ Si_{7/21}$
$G^{Q}_{m} - 3/21 \cdot {}^{\circ}G^{fcc\_A1}_{Al} - 2/21 \cdot {}^{\circ}G^{fcc\_A1}_{Cu} - 9/21 \cdot {}^{\circ}G^{hcp\_A3}_{Mg} - 7/21 \cdot {}^{\circ}G^{diamond\_A4}_{Si} = -17427.23 + 2.11 \cdot T$
S: $(Al, Si)_{0.5}\ Cu_{0.25}\ Mg_{0.25}$
${}^{\circ}G^{S}_{Si:Cu:Mg} - 0.5 \cdot {}^{\circ}G^{diamond\_A4}_{Si} - 0.25 \cdot {}^{\circ}G^{fcc\_Al}_{Cu} - 0.25 \cdot {}^{\circ}G^{hcp\_A3}_{Mg} = -2461 \cdot {}^{\circ}L^{S}_{Al,Si:Cu:Mg} = -10503.87$
τ_4-AlCuMn: $(Al, Si)_5\ Cu_2\ Mn_3$
${}^{\circ}G^{S}_{Si:Cu:Mg} - 0.5 \cdot {}^{\circ}G^{diamond\_A4}_{Si} - 0.2 \cdot {}^{\circ}G^{fcc\_Al}_{Cu} - 0.3 \cdot {}^{\circ}G^{cbcc\_A12}_{Mg} = -33005.45$
τ_9-AlMnSi: $Al_{14}\ (Cu, Mn)_4\ (Al, Si)_5$
${}^{\circ}G^{S}_{Al:Cu:Al} - 19/23 \cdot {}^{\circ}G^{fcc\_Al}_{Al} - 4/23 \cdot {}^{\circ}G^{fcc\_Al}_{Cu} = -545.34$
${}^{\circ}G^{S}_{Al:Cu:Si} - 14/23 \cdot {}^{\circ}G^{fcc\_Al}_{Al} - 4/23 \cdot {}^{\circ}G^{fcc\_A1}_{Cu} = -5/23 \cdot {}^{\circ}G^{diamond\_A4}_{Si} - 1398.17$

[a] In J mol-atoms^{-1}; temperature (T) in Kelvin. The Gibbs energies for the pure elements are from the compilation of Dinsdale [72].

to be hexagonal by Phragmen [53] using X-ray diffraction. However, the constitution of Q is controversial, which has been reported as $Al_4Cu_1Mg_5Si_4$ [45], $Al_xCu_4Mg_5Si_4$ [51,52], $Al_4Cu_2Mg_8Si_7$ [54], $Al_5Cu_2Mg_8Si_6$ [44,53,55], and $Al_xCu_2Mg_{12-x}Si_7$ [56]. Wolverton [57] calculated the enthalpies of formation for Q with different constitutions by using the first-principles calculations and demonstrated that $Al_3Cu_2Mg_9Si_7$ is the most stable form of Q. Thermodynamic data for the Q phase are not available in the literature.

Most recently, Yan [26] and Pan et al. [58] have modeled this quaternary system. However, their thermodynamic parameters for Q phase were obtained only based on the phase diagram data. Moreover, their calculated invariant reaction $L + Mg_2Si \leftrightarrow Q + (Al) + (Si)$ disagrees with the experimental one $(L + (Si) + Mg_2Si \leftrightarrow Q + (Al))$ [44]. Thus, a reassessment of this quaternary system is necessary in order to provide a reliable basis for thermodynamic calculations in related multi-component systems.

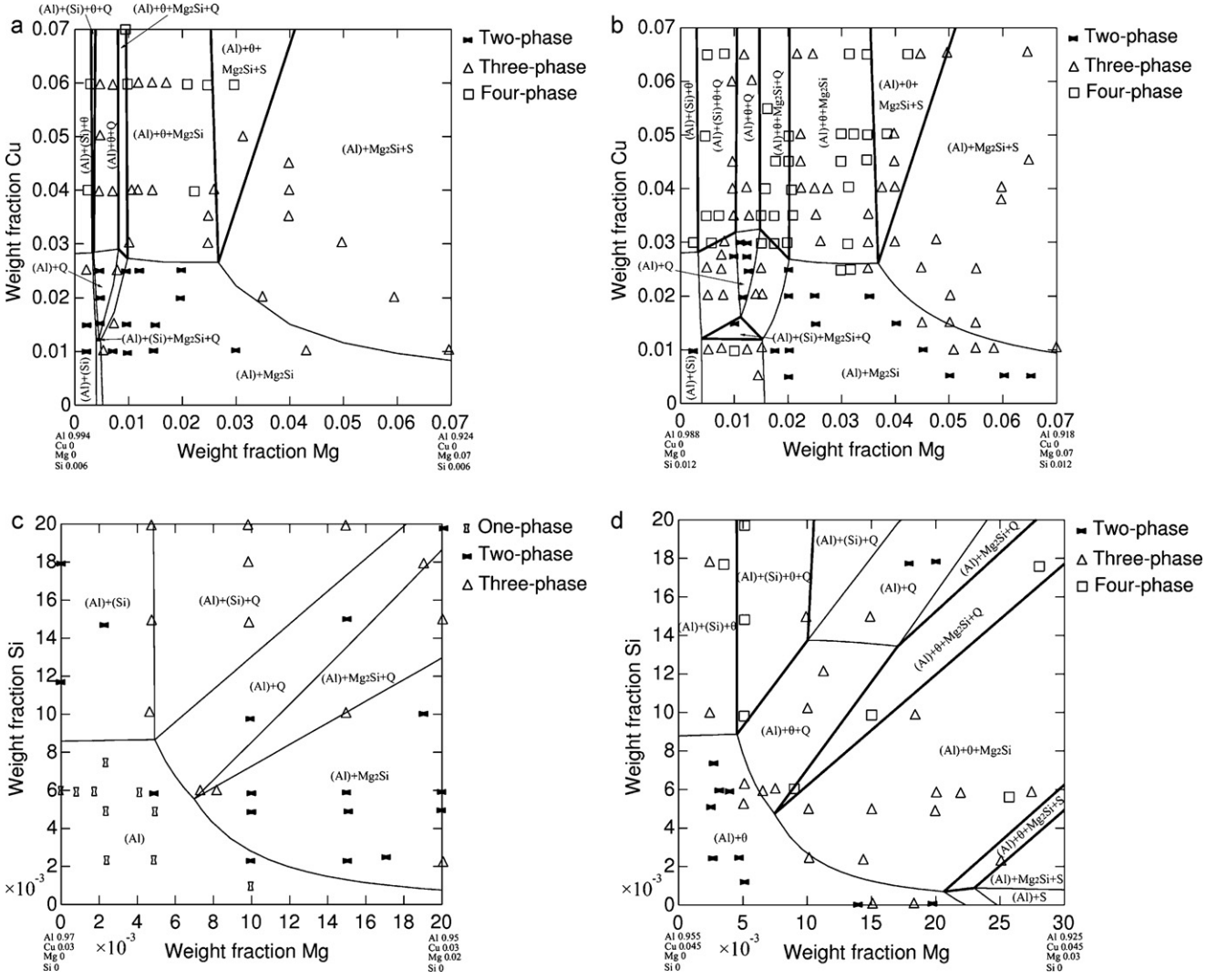

Fig. 2. Calculated isothermal sections in the Al–Cu–Mg–Si system along with the experimental data: (a) 0.6 wt.% Si at 460 °C (data from Axon [37]), (b) 1.2 wt.% Si at 460 °C (data from Axon [38]), (c) 3 wt.% Cu at 520 °C (data from Smith [30]) and (d) 4.5 wt.% Cu at 520 °C (data from Smith [30]).

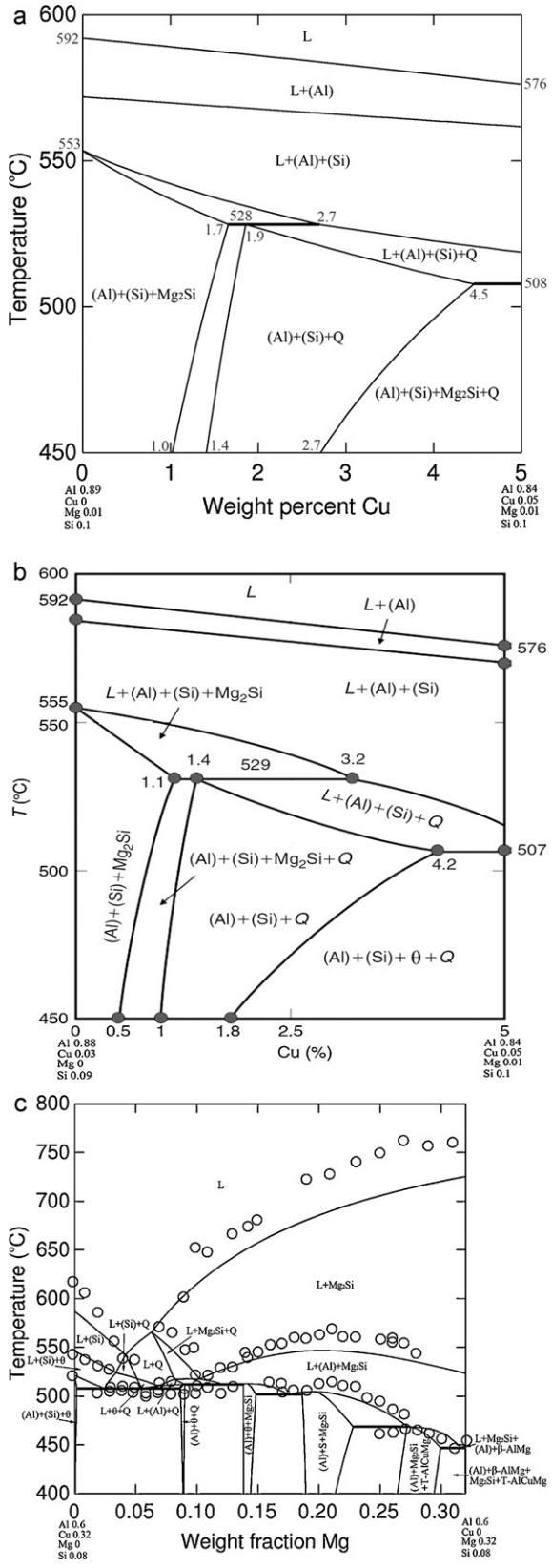

Fig. 3. Vertical sections in the Al–Cu–Mg–Si system: (a) calculated one with 1 wt.% Mg and 10 wt.% Si, (b) experimental one with 1 wt.% Mg and 10 wt.% Si [42] and (c) calculated one with 60 wt.% Al and 8 wt.% Si along with the experimental data from Petrov and Nagorskaya [36].

Table 4
Enthalpies of formation of Q phase computed by different methods.[a]

Q phase	Enthalpy of formation (kJ mol-atoms^{-1})	Method	Reference
$Al_5Cu_2Mg_8Si_6$	−12.0	FP(GGA)	[57]
	−12.9	FP(LDA)	[57]
	−12.5	FP(GGA)	This work
	−35.53	CALPHAD	[26]
	784.6	CALPHAD	[58]
$Al_3Cu_2Mg_9Si_7$	−16.1	FP(GGA)	[57]
	−17.4	FP(LDA)	[57]
	−17.5	FP(GGA)	[71]
	−17.6	FP(GGA)	This work
	−17.4	CALPHAD	This work

[a] FP, the first-principles calculations; GGA, the generalized gradient approximation; LDA, the local density approximation.

2.3.2. *The Al–Cu–Mn–Si system*

Information on the phase equilibria of the Al–Cu–Mn–Si system is very limited [44,53,59]. Phragmen [53] reported that τ_9-AlMnSi takes Cu into solid solution. Using optical microscopy, Bagchik and Axon [59] determined two isothermal sections in the Al-rich corner at 460 °C with the composition of 1 and 2 wt.% Mn. Their results also revealed that τ_4-AlCuMn and τ_9-AlMnSi dissolves a small amount of Si and Cu, respectively. Mondolfo [44] experimentally observed three invariant reactions in the Al-rich corner of the quaternary system. No quaternary phase is observed in the system [44,53,59]. No thermodynamic modeling has been performed for the quaternary system in the literature.

In the present work, the thermodynamic parameters for the phases τ_4-AlCuMn and τ_9-AlMnSi are evaluated by considering the phase diagram data [59] and the invariant reaction data [44].

2.3.3. *The Al–Cu–Mg–Mn, Al–Mg–Mn–Si, and Cu–Mg–Mn–Si systems*

No quaternary phases were reported in the Al–Cu–Mg–Mn, Al–Mg–Mn–Si and Cu–Mg–Mn–Si quaternary systems [53]. In the literature, there is no experimental information on the phase diagrams of the above three quaternary systems. Consequently, the thermodynamic properties for the above three quaternary systems are synthesized from the descriptions of the constituent ternary systems.

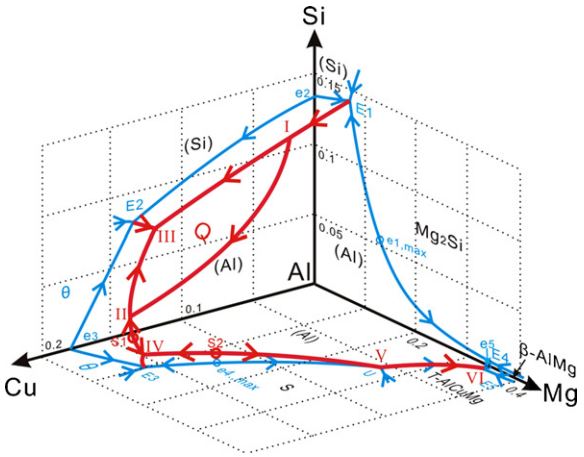

Fig. 4. Calculated liquidus projection of the Al–Cu–Mg–Si system in the Al-rich corner according to the present work. The compositions are given in weight fractions.

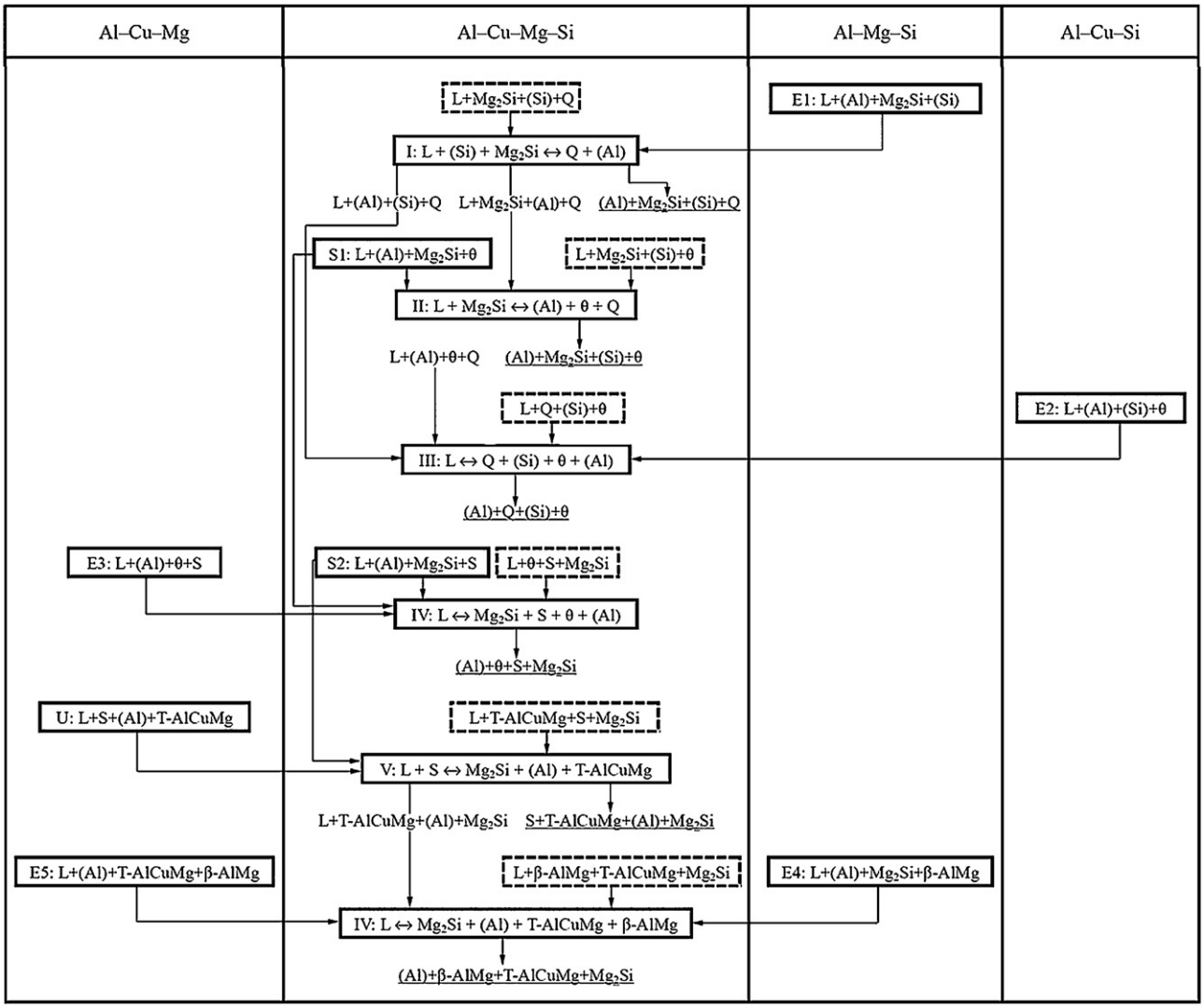

Fig. 5. Reaction scheme for the Al–Cu–Mg–Si system in the Al-rich corner according to the present work.

2.4. The Al–Cu–Mg–Mn–Si quinary system

Only five of the invariant reactions in the Al-rich corner of the quinary system have been reported by Mondolfo [44] using TA and microstructure observation techniques.

3. Enthalpy of formation for Q computed via first-principles method

In order to select the proper constitution for the present thermodynamic modeling and provide thermodynamic parameters with sound physical meaning, the first-principles calculations are used to determine the enthalpies of formation for Q in the Al–Cu–Mg–Si quaternary system.

We utilize the first-principles plane wave pseudopotential method, as implemented in the highly efficient Vienna ab initio simulation package (VASP) [60] to obtain the enthalpy of formation. The calculations are performed using the generalized gradient approximation (GGA) of Perdew [61]. Convergence tests indicated that 400 eV is a sufficient cutoff to insure total energy differences for the precipitates were less than 1 meV/atom. The atoms are relaxed toward equilibrium until the Hellmann–Feynman forces are less than 10^{-2} eV Å^{-1}. Brillouin zone integrations are performed using the Monkhorst–Pack *k*-point meshes scheme [62]. Both the unit cell sizes and the ionic coordinates are fully relaxed to obtain the equilibrium state.

The equilibrium enthalpy of formation $\Delta H^{eq}(A_pB_qC_sD_t)$ for the Q phase $A_pB_qC_sD_t$ is given by the energy of the phase relative to the composition-weighted average of the energies of the pure constituents each in their equilibrium crystal structures:

$$\Delta H^{eq}(A_pB_qC_sD_t) = E(A_pB_qC_sD_t) - [x_AE^{eq}(A) + x_BE^{eq}(B) + x_CE^{eq}(C) \quad x_DE^{eq}(D)] \tag{1}$$

where $E(A_pB_qC_sD_t)$, $E^{eq}(A)$, $E^{eq}(B)$, $E^{eq}(C)$ and $E^{eq}(D)$ are the energies (per atom) of the compound $A_pB_qC_sD_t$ and constituents, *A*, *B*, *C*, *D* each in their equilibrium (zero-pressure) geometries, $x_A = p/(p+q+s+t)$, $x_B = q/(p+q+s+t)$, $x_C = s/(p+q+s+t)$ and $x_D = t/(p+q+s+t)$ are the concentrations of *A*, *B*, *C*, and *D*, respectively. Different atomic occupations reported in the literature [53–58] for the Q phase $Al_5Cu_2Mg_8Si_6$, $Al_4Cu_2Mg_8Si_7$ and $Al_3Cu_2Mg_9Si_7$ are investigated in our calculations.

4. Thermodynamic models

Based on the present first-principles calculations which will be discussed in the following section, the quaternary phase Q is treated as a stoichiometric phase $Al_3Cu_2Mg_9Si_7$, and its Gibbs energy is

Table 5
Comparison of the calculated and measured invariant reaction temperatures for the invariant equilibria in Al-rich corner of the quaternary Al–Cu–Mg–Si system.

Point	Reaction	Measured T (°C)	Calculated T (°C)
I	$L+(Si)+Mg_2Si \leftrightarrow Q+(Al)$	529 [44]	528
		521 [36]	
		541.6 [43]	
II	$L+Mg_2Si \leftrightarrow (Al)+\theta+Q$	512 [44]	512
		512 [43]	
		512 [45]	
		510 [36]	
		510 [46]	
		513 [48]	
III	$L \leftrightarrow Q+(Si)+\theta+(Al)$	507 [44]	508
		507 [45]	
		507 [46]	
		507 [6]	
		505 [36]	
		509 [43]	
		510 [48]	
		510 [49]	
		510 [47]	
IV	$L \leftrightarrow Mg_2Si+S+\theta+(Al)$	500 [44]	502
		500 [36]	
		500 [46]	
		503 [47]	
		507 [45]	
V	$L+S \leftrightarrow Mg_2Si+(Al)+$T-AlCuMg	467 [44]	469
		464 [36]	
		471 [43]	
VI	$L \leftrightarrow Mg_2Si+(Al)+$T-AlCuMg$+\beta$-AlMg	444–448 [44]	447
		444 [36]	
		449 [43]	
		450 [47]	

expressed relative to the mechanical mixing of the pure elements by the following equation

$$G_m^Q - H^{SER} = 3 \cdot^\circ G_{Al}^{fcc\_Al} + 2 \cdot^\circ G_{Cu}^{fcc\_Al} + 9 \cdot^\circ G_{Mg}^{hcp\_A3} + 7 \cdot^\circ G_{Si}^{diamond\_A4} + A + B \cdot T \quad (2)$$

in which the coefficients A and B are to be evaluated.

In view of the solubility for Si in the S phase [63,64], this phase is described with the sublattice model $(Al, Si)_2Cu_1Mg_1$. According to the formula for sublattice model [65,66], the Gibbs energy of S phase per mole-formula can be expressed as:

$$^\circ G^S - H^{SER} = y'_{Al} \cdot^\circ G^S_{Al:Cu:Mg} + y'_{Si} \cdot^\circ G^S_{Si:Cu:Mg} + 2RT(y'_{Al} \cdot \ln y'_{Al} + y'_{Si} \cdot \ln y'_{Si}) + y'_{Al} \cdot y'_{Si} \cdot^\circ L^S_{Al,Si:Cu:Mg} + y'_{Al} \cdot y'_{Si} \cdot (y'_{Al} - y'_{Si}) \cdot {}^1L^S_{Al,Si:Cu:Mg} + \ldots \quad (3)$$

where the two parameters denoted $^\circ G^S_{*:Cu:Mg}$ (also called compound energies) are expressed relative to the Gibbs energies of pure Al, Cu, Mg, and Si at the same temperature. The superscript $'$ means the first sublattice of the model $(Al, Si)_2Cu_1Mg_1$.

The equations similar to Eq. (3) can be written for the Gibbs energies of τ_1-AlCuMn and τ_9-AlMnSi, which are modeled as $(Al, Si)_5Cu_3Mn_2$ and $Al_{14}(Cu, Mn)_4(Al, Si)_5$, respectively.

Table 6
Comparison between calculated and measured reaction temperatures for the invariant equilibria in Al-rich part of the quaternary Al–Cu–Mn–Si system.

Reaction	Measured T (°C) [44]	Calculated T (°C) (this work)
$L \leftrightarrow (Al)+(Si)+\theta+\tau_9$-AlMnSi	597	606
$L+\tau_1$-AlCuMn $\leftrightarrow (Al)+\theta+\tau_9$-AlMnSi	547	541
$L+Al_6Mn \leftrightarrow (Al)+\tau_1$-AlCuMn$+\tau_9$-AlMnSi	517	521

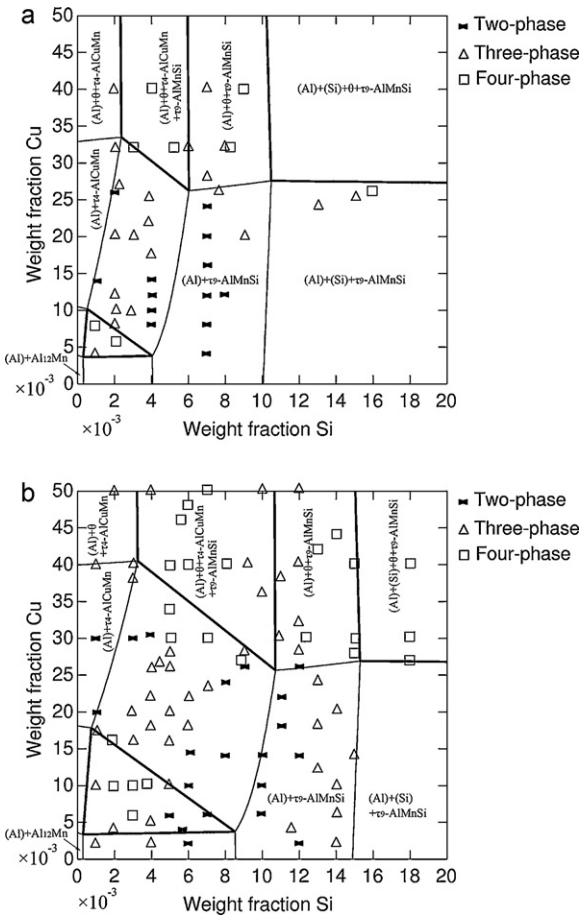

Fig. 6. Calculated isothermal sections in the Al–Cu–Mn–Si system at 460 °C along with the experimental data from Bagchik and Axon [59] with: (a) 1 wt.% Mn and (b) 2 wt.% Mn.

Table 7
Comparison between calculated and measured reaction temperatures for the invariant equilibria in Al-rich part of the quinary Al–Cu–Mg–Mn–Si system.

Reaction	Measured T (°C) [44]	Calculated T (°C) (this work)
$L+(Si)+Mg_2Si \leftrightarrow (Al)+Q+\tau_9$-AlMnSi	528	528
$L+Mg_2Si \leftrightarrow (Al)+\theta+Q+\tau_9$-AlMnSi	511	512
$L \leftrightarrow (Al)+(Si)+\theta+Q+\tau_9$-AlMnSi	505	507
$L+\tau_9$-AlMnSi $\leftrightarrow (Al)+Mg_2Si+\theta+\tau_1$-AlCuMn	502	502
$L \leftrightarrow (Al)+Mg_2Si+S+\theta+\tau_9$-AlMnSi	500	501

5. Results and discussion

5.1. The Al–Cu–Mg–Si system

The thermodynamic optimization was performed by means of the PARROT program [67]. In order to reproduce the experimentally measured phase equilibria in the Al-rich sides of the Al–Cu–Mg system [30], one regular interaction parameter for the fcc_A1 phase is adjusted: $^\circ L^{fcc}_{Al,Cu,Mg} = -60$ kJ mol-atoms^{-1}. Table 2 compares the calculated and observed invariant equilibria in Al-rich corner of Al–Cu–Mg system, showing a good agreement. The liquidus projections of the ternary Al–Cu–Mg, Al–Cu–Si [32] and Al–Mg–Si [33] systems in the Al-rich corner are calculated using the present database, as shown in Fig. 1.

As indicated in the preceding section, it is of interest to reassess the Al–Cu–Mg–Si quaternary system. The present first-principles calculations show that the enthalpies of formation for $Al_5Cu_2Mg_8Si_6$, $Al_4Cu_2Mg_8Si_7$ and $Al_3Cu_2Mg_9Si_7$ phases are −12.5,

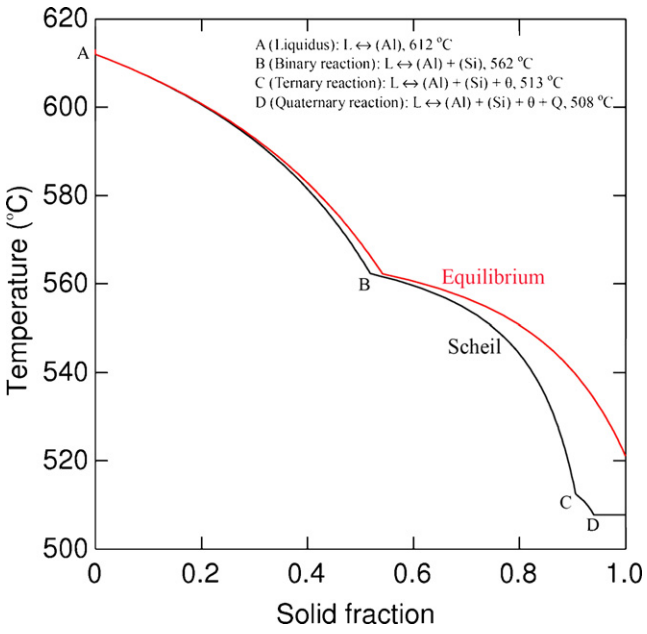

Fig. 7. Calculated equilibrium and Gulliver–Scheil non-equilibrium solidification curves of Al alloy B319.1.

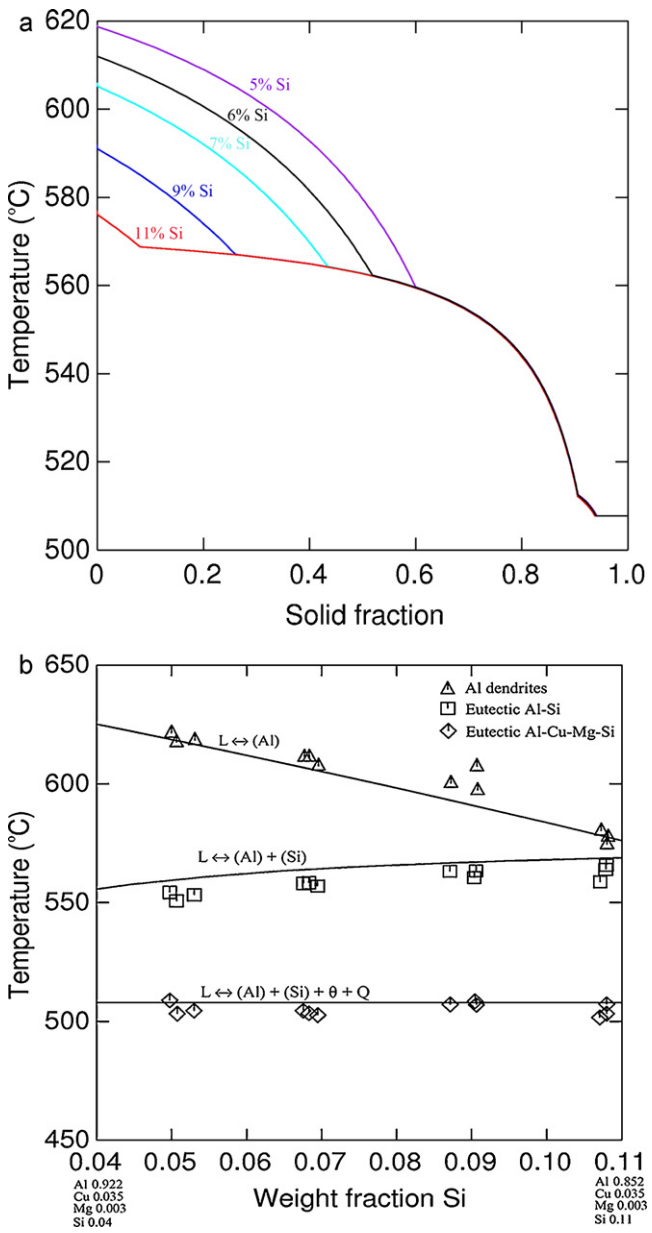

Fig. 8. Effect of Si contents on the solidification behavior of alloy B319.1 (90.2Al–6Si–3.5Cu–0.3Mg, in wt.%) under the Gulliver–Scheil non-equilibrium condition: (a) calculated solidification curves of Al alloys (96.2 – *x*)Al–*x*Si–3.5Cu–0.3Mg (*x* = 5, 6, 7, 9 and 11, in wt.%); (b) calculated reaction temperatures of Al alloys (96.2 – *x*)Al–*x*Si–3.5Cu–0.3Mg (*x* = 5, 6, 7, 9 and 11, in wt.%) during solidification process with experimental data [77].

−14.1, and −17.6 kJ mol-atoms^{-1}, respectively. Our results are consistent with those of Wolverton [57] and Ravi and Wolverton [71], indicating that the most stable form of Q is $Al_3Cu_2Mg_9Si_7$. Thus, $Al_3Cu_2Mg_9Si_7$ is selected as the model of Q, and its enthalpy of formation is set as the start value for the *A* parameter of the Q phase. Then, the *A* and *B* parameters of the Q phase are optimized based on the measured invariant phase equilibria [6,36,43–49]. Finally, the parameters of the S phase are adjusted by considering the phase diagram data [36–42]. The optimized thermodynamic parameters in the Al–Cu–Mg–Si quaternary system are listed in Table 3.

The data for the enthalpy of formation of Q calculated in the present work and by the other researchers with different methods are summarized in Table 4. It can be clearly seen that the present CALPHAD results are more reasonable than those of Yan [26] and Pan et al. [58]. The CALPHAD calculated value from Pan et al. [58] is too positive while that from Yan [26] is too negative, in comparison with the first-principles calculated values. The value of 784.6 kJ mol-atoms^{-1} may be misprinted in Ref. [58]. We cannot find out the exact value which Pan et al. [58] used for their thermodynamic calculations.

Fig. 2 shows four calculated isothermal sections in the Al-rich corner of the Al–Cu–Mg–Si system along with the experimental data [30,37,38]. One calculated vertical section with 1 wt.% Mg and 10 wt.% Si is compared with the experimental one [42], as presented in Fig. 3a and b. It is demonstrated that the experimental data are reasonably described by the thermodynamic calculation. Fig. 3c shows one calculated vertical section with 60 wt.% Al and 8 wt.% Si along with the experimental data from Petrov and Nagorskaya [36]. Most of the experimental data are accurately reproduced by the present database, except for those at high temperatures. The reason is that the parameters of the constituent ternary Al–Cu–Si [32] and Al–Mg–Si [33] systems cannot describe the experimental data [36] well enough. Calculations were also performed for the experimental phase diagrams reported in the literature [30,36,39–41], also showing good agreement. The representative results are given in supplementary material (Supplementary Figs. 1 and 2).

The calculated liquidus projections are shown in Fig. 4 and the correspondingly calculated invariant reactions are presented in Table 5. Again, the calculated results agree reasonably with the experimental data [6,36,43–49]. Specially, the peritectic reaction $L + (Si) + Mg_2Si \leftrightarrow Q + (Al)$ is well reproduced by the present database. The reaction scheme for the quaternary system in the Al-rich corner is constructed, as shown in Fig. 5.

5.2. The Al–Cu–Mn–Si system

The optimized thermodynamic parameters in the Al–Cu–Mn–Si quaternary system are listed in Table 3. Fig. 6 shows the calculated isothermal sections in the Al-rich corner along with the experimental data from Bagchik and Axon [59]. The fit to the experimental data is reasonable. A further check on the reliability of the thermodynamic modeling is provided in Table 6, where the calculated and observed [44] temperatures for the invariant reactions are presented, showing a reasonable agreement.

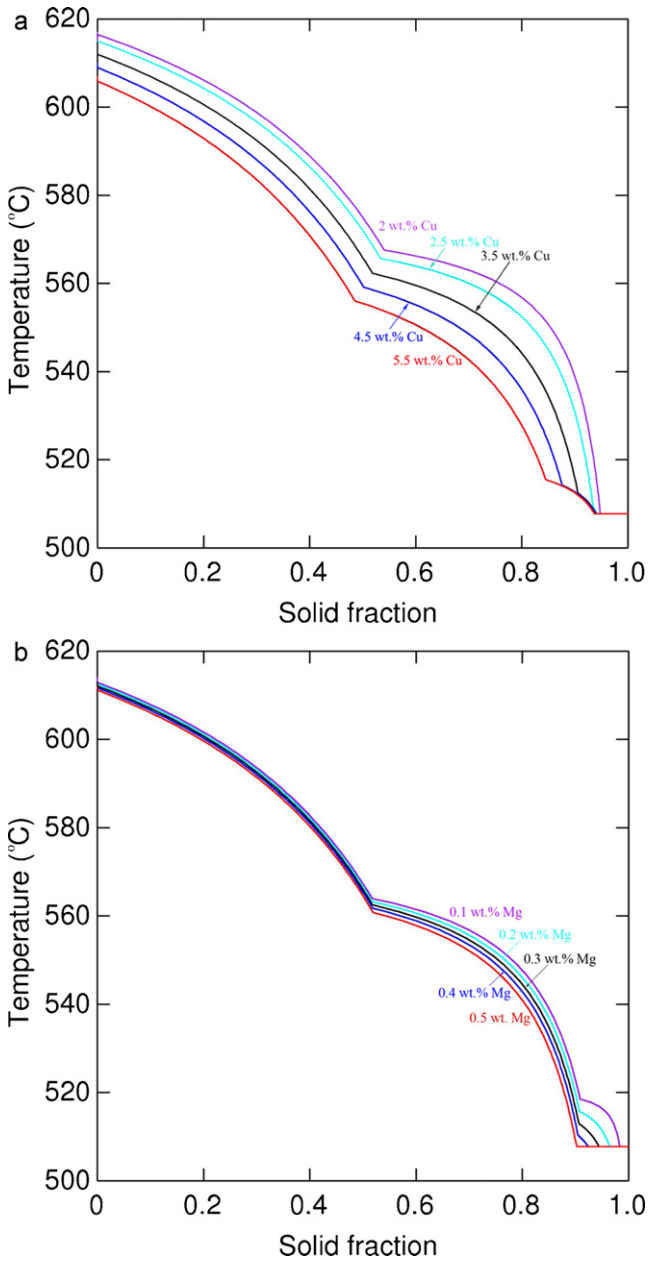

Fig. 9. Calculated solidification curves of Al alloys under the Gulliver–Scheil condition: (a) (93.7 – *x*)Al–6Si–*x*Cu–0.3Mg (*x* = 2, 2.5, 3.5, 4.5 and 5.5, in wt.%); (b) (90.5 – *x*)Al–6Si–3.5Cu–*x*Mg (*x* = 0.1, 0.2, 0.3, 0.4 and 0.5, in wt.%).

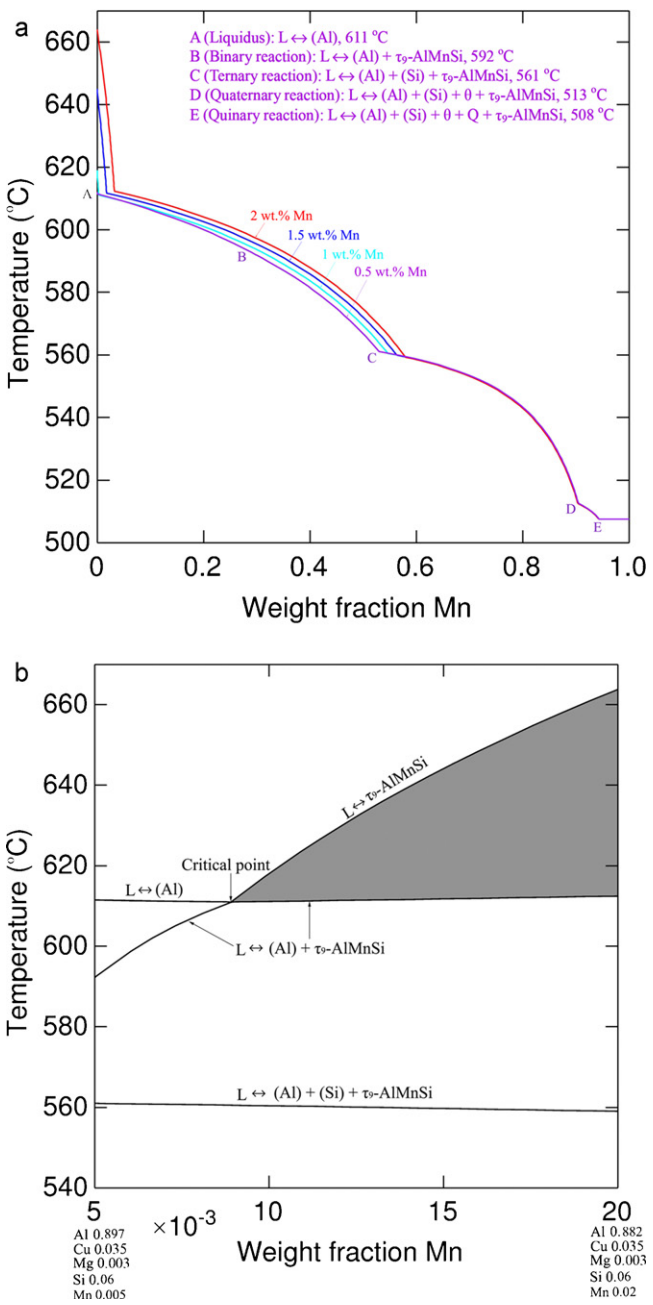

Fig. 10. Effect of Mn addition on the solidification behavior of Al alloy B319.1 (90.2Al–6Si–3.5Cu–0.3Mg, in wt.%) under the Gulliver–Scheil condition: (a) calculated solidification curves of Al alloys (90.2 – *x*)Al–6Si–3.5Cu–0.3Mg–*x*Mn (*x* = 0.5, 1, 1.5 and 2, in wt.%); (b) calculated liquidus and reaction temperatures of Al alloys (90.2 – *x*)Al–6Si–3.5Cu–0.3Mg–*x*Mn (*x* = 0.5, 1, 1.5 and 2, in wt.%) during solidification process. The gray region shows where sedimentation of primary τ_9-AlMnSi precipitates occurs.

5.3. The Al–Cu–Mg–Mn–Si system

A thermodynamic database for the Al–Cu–Mg–Mn–Si system is established on the basis of the constituent binary, ternary and quaternary systems. Table 7 lists the calculated and experimental [44] invariant reactions, showing a good agreement between the reactions.

5.4. Solidification simulation of Al alloys

Various approximations and simplifications are always needed in simulating the complicated solidification process [15]. One qualitative approximation is to use the Gulliver–Scheil model [73,74]. It has been realized that there is a reasonable agreement between prediction and experiment by applying the model to the description of solidification process [15,75]. In the present work, Gulliver–Scheil simulations are performed to describe the solidification behaviors of Al alloys B319.1 (90.2Al–6Si–3.5Cu–0.3Mg, in wt.%) and B319.1 + *x*Mn (*x* = 0.5–2, in wt.%).

Solidification simulation of Al alloy B319.1 (90.2Al–6Si–3.5Cu–0.3Mg, in wt.%) is conducted to further verify reliability of the established Al–Cu–Mg–Mn–Si thermodynamic database. Fig. 7 shows the calculated equilibrium and non-equilibrium Gulliver–Scheil solidification curves of the alloy. Only two reactions are detected for the equilibrium curve while four reactions corresponding to the Gulliver–Scheil curve are detected, as shown in Fig. 7. The microstructure of the solidified

Table 8
Calculated reaction temperatures of Al alloys (93.7 − *x*)Al–6Si–*x*Cu–0.3Mg (*x* = 2, 2.5, 3.5, 4.5 and 5.5, in wt.%) and (90.5 − *x*)Al–6Si–3.5Cu–*x*Mg (*x* = 0.1, 0.2, 0.3, 0.4 and 0.5, in wt.%) during solidification process.

Element	Composition (wt.%)	Liquidus, *T* (°C)	Binary reaction, *T* (°C)	Ternary reaction, *T* (°C)	Quaternary reaction, *T* (°C)
Cu	5.5	606	556	516[a]	508
	4.5	609	559	514[a]	508
	3.5	612	562	513[a]	508
	2.5	615	566	510[a]	508
	2.1	616	567	508[a]	508
	2	616	567	508[b]	508
	1.9	616	567	508[b]	508
Mg	0.1	613	564	518[a]	508
	0.2	612	563	516[a]	508
	0.3	612	562	513[a]	508
	0.4	612	562	510[a]	508
	0.49	611	561	508[a]	508
	0.5	611	561	508[b]	508
	0.51	611	561	508[b]	508

[a] Temperature for ternary reaction L ↔ (Al) + (Si) + θ.
[b] Temperature for ternary reaction L ↔ (Al) + (Si) + Q.

alloy resulting from the Gulliver–Scheil model is (Al) + (Si) + θ + Q, which is identical to the generally observed one [76,77]. However, the microstructure according to equilibrium solidification calculation is (Al) + (Si), which is significantly different from the observed one [76,77]. Fig. 8a shows the calculated solidification curves with different Si contents of alloy B319.1 under the Gulliver–Scheil condition. As it can be seen, when Si content increases, the liquidus temperature decreases and the binary reaction temperature increases but the last two reactions remain the same. This is also shown in Fig. 8b, in which the calculated reaction temperatures are compared with the experimental data [77]. The excellent agreement is an additional evidence for the reliability of the present thermodynamic database for the Al–Cu–Mg–Si quaternary system. Also, we can conclude from Fig. 8 that different B319.1 alloys with Si contents (5–11 wt.%) go through the same reactions during the solidification process.

We apply the present thermodynamic database to predict effects of Cu and Mg contents on the solidification behavior of Al alloy B319.1. Fig. 9 shows the calculated solidification curves of B319.1 alloy with different Cu and Mg contents under the Gulliver–Scheil condition. Compared to Si, both Cu and Mg influence the ternary reaction temperatures apparently. Table 8 summarizes effects of Cu and Mg contents on the reaction temperatures. As Cu content decreases or Mg content increases, the calculations show that the transition of the ternary reaction occurs at the composition of 2 wt.% Cu or 0.5 wt.% Mg. Thus, our results demonstrate that the contents of Cu and Mg should be >2 wt.% and <0.5 wt.%, respectively, in order to maintain the same solidification reactions as those for Al alloy B319.1 (90.2Al–6Si–3.5Cu–0.3Mg, in wt.%).

In order to explain the effect of Mn addition on the properties of Al alloys, the present database is utilized to study the solidification behavior of Al alloys B319.1 + *x*Mn (*x* = 0.5–2, in wt.%). Compared to the solidification curves of B319.1 (90.2Al–6Si–3.5Cu–0.3Mg, in wt.%) in Fig. 7, τ_9-AlMnSi takes part in the reactions during the solidification process, as shown in Fig. 10. The microstructure obtained from the alloys is (Al) + (Si) + θ + Q + τ_9-AlMnSi. It can be concluded that the increase in strength of the Al–Cu–Mg–Si alloys with the addition of Mn [8] is due to the formation of τ_9-AlMnSi phase. As it can be seen from Fig. 10a, the liquidus of B319.1 decreases slightly when 0.5 wt.% Mn is added, but increases significantly when 1, 1.5 and 2 wt.% Mn are added. This phenomenon can be explained by transition of the liquidus reactions and one critical point at 0.89 wt.% Mn is detected, as shown in Fig. 10b. For Al alloys B319.1 + *x*Mn (*x* > 0.89, in wt.%), sedimentation of primary τ_9-AlMnSi precipitates occurs [76,78] in the gray region of Fig. 10b. This phenomenon is commonly known in the die casting field as "sludge" or "fallout" [79], which is harmful to Al alloys. Thus, the present work demonstrates that the Mn content should be less than 0.89 wt.% for Al alloy B319.1 in order to maintain the good properties of the alloy.

6. Conclusions

- The enthalpy of formation for the quaternary phase Q in the Al–Cu–Mg–Si system is computed by means of the first-principles calculations. Based on the first-principles generated data and the experimental information, thermodynamic parameters for the Q phase are obtained by using the CALPHAD approach. Compared with previous assessments, the present CALPHAD calculations are consistent with the first-principles generated data.
- The thermodynamic database for the quinary Al–Cu–Mg–Mn–Si system is obtained based on the constituent binary, ternary, and quaternary systems. Particularly, the phase equilibria in the Al-rich corner of the quaternary Al–Cu–Mg–Si and Al–Cu–Mn–Si systems are modeled in detail. The reliability of the established database is verified by good agreement between calculation and experiment for phase diagrams, invariant reactions and Gulliver–Scheil non-equilibrium solidification behaviors.
- Gulliver–Scheil non-equilibrium solidification behaviors of Al alloys B319.1 (90.2Al–6Si–3.5Cu–0.3Mg, in wt.%) and B319.1 + *x*Mn (*x* = 0.5–2, in wt.%) are investigated. The application of the presently thermodynamic database to control phase transitions throughout solidification process for Al alloys indicates the importance of thermodynamic databases in material design.

Acknowledgements

The financial support from National Basic Research Program of China (2011CB610401) and the National Natural Science Foundation of China (Grant nos. 50971135, 50831007 and 50721003) is acknowledged. Li Chen thanks National Natural Science Foundation for Youth of China (Grant No. 51001120).

Appendix A. Supplementary data

Supplementary data associated with this article can be found, in the online version, at doi:10.1016/j.tca.2010.11.009.

References

[1] C.D. Lee, Mater. Sci. Eng., A 527 (2010) 3144–3150.

[2] M. Gaffar, A. Gaber, M. Mostafa, E. Abozeid, Mater. Sci. Eng., A 465 (2007) 274–282.
[3] D.J. Chakrabarti, D.E. Laughlin, Prog. Mater. Sci 49 (2004) 389–410.
[4] D.J. Chakrabarti, B.K. Cheong, D.E. Laughlin, in: S.K. Das (Ed.), Automotive Alloys II, Proceedings of the Symposium Presented at the TMS Annual Meeting San Antonio, 1998, pp. 27–44.
[5] L. Lasa, J.M. Rodriguez-Ibabe, Mater. Sci. Eng., A 363 (2003) 193–202.
[6] G. Wang, X. Bian, W. Wang, J. Zhang, Mater. Lett. 57 (2003) 4083–4087.
[7] A. Hekmat-Ardakan, F. Ajersch, Acta Mater. 58 (2010) 3422–3428.
[8] J.R. Davis, Aluminum and Aluminum Alloys, ASM International Handbook Committee, 1993.
[9] D. Liu, H.V. Atkinson, H. Jones, Acta Mater. 53 (2005) 3807–3819.
[10] Q. Zeng, Y. Wen, J. Xiong, Hot Working Technol. 38 (2009) 26–31.
[11] Z. Zhu, Ph.D. Thesis, University of Southampton, UK, 2006.
[12] N.A. Belov, D.G. Eskin, A.A. Aksenov, Multicomponent Phase Diagrams: Applications for Commercial Aluminum Alloys, Elsevier Science, 2005.
[13] J. Lacaze, G. Lesoult, in: J.A. Sekhar, J. Dantzig (Eds.), Nature and Properties of Semi-Solid Materials, TMS, Warrendale, Pennsylvania, USA, 1991.
[14] J.E. Hatch, Aluminum Properties and Physical Metallurgy, American Society for Metals, Ohio, 1984.
[15] Y. Du, Y.A. Chang, S. Liu, B. Huang, F.-Y. Xie, Y. Yang, S.-L. Chen, Z. Metallkd. 96 (2005) 1–12.
[16] C. Wolverton, X.-Y. Yan, R. Vijayaraghavan, V. Ozolins, Acta Mater. 50 (2002) 2187–2197.
[17] L. Zhang, J. Wang, Y. Du, R. Hu, P. Nash, X.-G. Lu, C. Jiang, Acta Mater. 57 (2009) 5324–5341.
[18] Y. Du, L. Li, J. Wang, J. Wang, Z. Jin, CALPHAD 33 (2009) 719–722.
[19] W. Sun, Y. Du, Y. Kong, H. Xu, W. Xiong, S. Liu, Int. J. Mater. Res. 100 (2009) 59–67.
[20] N. Saunders, in: I. Ansara, A.T. Dinsdale, M.H. Rand (Eds.), COST 507-Thermochemical Database for Light Metal Alloys, vol. 2, Office for Official Publications of the European Communities, Luxembourg, 1998, pp. 28–33.
[21] P. Liang, H.-L. Su, P. Donnadieu, M.G. Harmelin, A. Quivy, P. Ochin, G. Effenberg, H.J. Seifert, H.L. Lukas, F. Aldinger, Z. Metallkd. 89 (1998) 536–540.
[22] Y. Du, J. Wang, J.R. Zhao, J.C. Schuster, R. Schmid-Fetzer, M. Ohno, Z.-K. Liu, S. Shang, H. Xu, W. Zhang, Int. J. Mater. Res. 98 (2007) 858–871.
[23] J. Gröbner, H.L. Lukas, F. Aldinger, CALPHAD 20 (1996) 247–254.
[24] C.A. Coughanowr, I. Ansara, R. Luoma, M. Hämäläinen, H.L. Lukas, Z. Metallkd. 82 (1991) 574–581.
[25] C.Y. He, Y. Du, H. Chen, S. Liu, H. Xu, Y. Ouyang, Z.-K. Liu, J. Alloys Compd. 457 (2008) 233–238.
[26] X.Y. Yan, Ph.D. Thesis, University of Wisconsin-Madison, USA, 2001.
[27] J. Gröbner, D. Mirkovic, M. Ohno, R. Schmid-Fetzer, J. Phase Equilib. 26 (2005) 234–239.
[28] D. Kevorkov, R. Schmid-Fetzer, J. Phase Equilib. 25 (2004) 140–151.
[29] Y. Du, J.C. Schuster, F. Weitzer, N. Krendelsberger, B. Huang, Z. Jin, W.P. Gong, Z. Yuan, H.H. Xu, Metall. Mater. Trans. A 35A (2004) 1613–1628.
[30] D.P. Smith, Metallurgia 63 (1962) 223–230.
[31] C.Y. He, Ph.D. Thesis, Central South University, China, 2008.
[32] C.Y. He, Y. Du, H.-L. Chen, H. Xu, CALPHAD 33 (2009) 200–210.
[33] H. Feufel, T. Goedecke, H.L. Lukas, F. Sommer, J. Alloys Compd. 247 (1997) 31–42.
[34] Y. Du, J.C. Schuster, F. Weitzer, N. Krendelsberger, B. Huang, Z. Jin, W.P. Gong, Z. Yuan, H. Xu, Metall. Mater. Trans. A 35A (2004) 1613–1628.
[35] S.H. Liu, Ph.D. Thesis, Central South University, China, 2010.
[36] D.A. Petrov, N.D. Nagorskaya, Zh. Obshch. Khim. 19 (1949) 1994–2037.
[37] H.J. Axon, J. Inst. Met. 81 (1952) 209–213.
[38] H.J. Axon, J. Inst. Met. 81 (1952) 449–450.
[39] H.J. Axon, J. Inst. Met. 83 (1955) 490–492.
[40] L.A. Willey, Aluminium, Alcoa Technical Center, Philadelphia, 1967.
[41] J. Crowther, J. Inst. Met. 76 (1949) 201–236.
[42] V.S. Zolotorevsky, N.A. Belov, M.V. Glazoff, Casting Aluminum Alloys, Alcoa Technical Center, Philadelphia, 2007.
[43] A. Schrader, Metall. Mater. Trans. A 3 (1949) 110–115.
[44] L.F. Mondolfo, Aluminum Alloys: Structure and Properties, Butterworths, Boston, 1976.
[45] J. Lacaze, G. Lesoult, O. Relave, I. Ansara, J.P. Riquet, Z. Metallkd. 78 (1987) 141–150.
[46] H.W.L. Phillips, Aluminium Devel. Ass., Inf. Bull. 25, London, 1961.
[47] J.L. Murray, J. Chim. Phys. 90 (1993) 151–166.
[48] D.J. Chakrabarti, J.L. Murray, Mater. Sci. Forum 177 (1996) 217–222.
[49] L. Lasa, J.M. Rodriguez-Ibabe, Mater. Charact. 48 (2002) 371–378.
[50] E.H. Dix Jr., G.F. Sager, B.P. Sager, Trans. AIME 99 (1932) 119–131.
[51] D.A. Petrov, Zh. Fiz. Khim. 9 (1937) 522–527.
[52] D.A. Petrov, Acta Phys.-Chim. URSS 6 (1937) 505–512.
[53] G. Phragmen, J. Inst. Met. 77 (1950) 489–552.
[54] R. Yassar, D. Field, H. Weiland, Scr. Mater. 53 (2005) 299–303.
[55] R.X. Li, R.D. Li, Y.H. Zhao, L.Z. He, C.X. Li, H.R. Guan, Z.O. Hu, Mater. Lett. 58 (2004) 2096–2101.
[56] L. Arnberg, B. Aurivillius, Acta Chem. Scand. 34 (1980) 1–5.
[57] C. Wolverton, Acta Mater. 49 (2001) 3129–3142.
[58] X. Pan, J. Morral, H. Brody, J. Phase Equilib. Diffus. 31 (2010) 144–148.
[59] A.P. Bagchik, H.J. Axon, J. Inst. Met. 83 (1954) 176–180.
[60] G. Kresse, J. Furthmueler, Phys. Rev. B 54 (1996) 11169–11186.
[61] J.P. Perdew, in: P. Ziesche, H. Eschrig (Eds.), Electronic Structure of Solids, Akademie Verlag, Berlin, 1991.
[62] H.J. Monkhorst, J.D. Pack, Phys. Rev. B 13 (1976) 5188–5192.
[63] D.G. Eskin, J. Mater. Sci. 38 (2003) 279–290.
[64] C.R. Hutchinson, S.P. Ringer, Metall. Mater. Trans. A 37A (2000) 2721–2733.
[65] M. Hillert, L.-I. Staffansson, Acta Chem. Scand. 24 (1970) 3618–3626.
[66] B. Sundman, J. Ágren, J. Phys. Chem. Solids 24 (1981) 297–301.
[67] B. Sundman, B. Jansson, J.-O. Andersson, CALPHAD 9 (1985) 153–190.
[68] A.I. Beljaew, Metallovedenic Aluminija, Metallurgia, Moscow, 1983.
[69] H.W. Phillips, Institute of Metals Monograph 25, Institute of Metals, London, 1959.
[70] A. Prince, G. Effenberg, Aluminium–Copper–Magnesium, in: G. Petzow, G. Effenberg (Eds.), Ternary Alloys, vol. 4, VCH Verlagsges, Weinheim, 1991.
[71] C. Ravi, C. Wolverton, Acta Mater. 52 (2004) 4213–4227.
[72] A.T. Dinsdale, CALPHAD 15 (1991) 317–425.
[73] G.H. Gulliver, J. Inst. Met. 9 (1913) 120–157.
[74] E. Scheil, Z. Metallkd. 34 (1942) 70–72.
[75] B. Jansson, M. Schalin, B. Sundman, J. Phase Equilib. 14 (1993) 557–562.
[76] L. Bäckerud, G. Chai, J. Tamminen, Solidification Characteristics of Aluminum Alloys Foundry Alloys, vol. 2, AFS/Skanaluminium, Sweden, 1990.
[77] A.A. Canales, J. Talamantes-Silva, D. Gloria, S. Valtierra, R. Colás, Thermochim. Acta 510 (2010) 82–87.
[78] J. Goberecht, Teil, Geißerei 62 (1975) 263–266.
[79] J.L. Jorstad, Die Casting Engineer, CRC Press, 1986.